Nanoscale

Accepted Manuscript

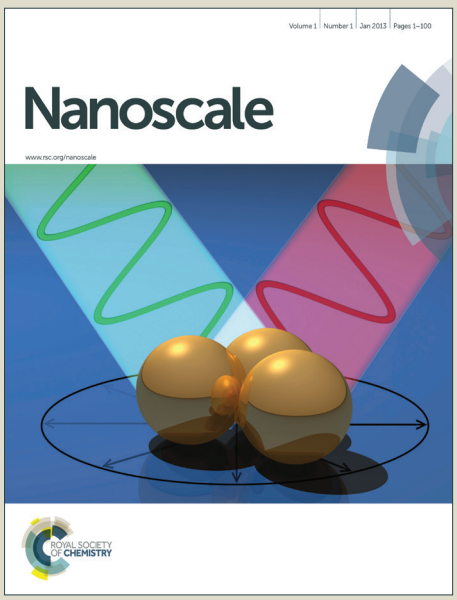

ROYAL SOCIETY OF CHEMISTRY

www.rsc.org/nanoscale

Cooperation between adsorbates accounts for the activation of atomic layer deposition reactions

Mahdi Shirazi and Simon D. Elliott*

Tyndall National Institute, University College Cork, Lee Maltings, Cork, Ireland

E-mail: simon.elliott@tyndall.ie

Phone: +353 (0)21 2346392. Fax: +353 (0)21 4904058

Abstract

Atomic layer deposition (ALD) is a technique for producing conformal layers of nanometre-scale thickness, used commercially in non-planar electronics and increasingly in other high-tech industries. ALD depends on self-limiting surface chemistry but the mechanistic reasons for this are not understood in detail. Here we demonstrate, by first-principle calculations of growth of HfO_2 from $Hf(N(CH_3)_2)_4/H_2O$ and $HfCl_4/H_2O$ and growth of Al_2O_3 from $Al(CH_3)_3/H_2O$, that, for all these precursors, co-adsorption plays an important role in ALD. By this we mean that previously-inert adsorbed fragments can become reactive once sufficient numbers of molecules adsorb in their neighbourhood during either precursor pulse. Through the calculated activation energies, this 'cooperative' mechanism is shown to have a profound influence on proton transfer and ligand desorption, which are crucial steps in the ALD cycle. Depletion of reactive species and increasing coordination cause these reactions to self-limit during one precursor pulse, but to be re-activated via the cooperative effect in the next pulse. This explains the self-limiting nature of ALD.

*To whom correspondence should be addressed

Introduction

The operation of nanoscale devices can depend on the chemical identity or morphology of a single layer of atoms in a 2D material or at an interface.[1–3] Preparing material interfaces with such atomic-scale control is a substantial challenge. One step towards this goal would be understanding the reactivity of surfaces towards particular reagents, and how to turn reactivity on and off at the level of single atomic layers.

ALD shows great promise in achieving monolayer-by-monolayer materials growth[4] and is already used commercially to fabricate layers of high-permittivity dielectric just a few nanometres thick in nanoelectronic transistors and memory devices.[5] As a type of chemical vapour deposition (CVD), material is deposited on a surface from gaseous precursor chemicals, typically one for each element of a binary compound. However, unlike other forms of CVD, ALD achieves atomic-level control because the reactions of each precursor gas self-terminate once the surface is saturated with one monolayer of precursor fragments. The surface is then inert. Growth resumes when the second precursor re-activates the surface and eliminates remaining ligands until saturation is again obtained. The sequential exposure to two precursor gases, separated by purges, completes one ALD cycle.

Despite remarkable achievements in characterising these sub-nanometre thin layers during exposure[6,7] and *in situ* to the reactor,[8] there is still little understanding of the crucial processes of saturation and re-activation. This is hampering progress in the field. For instance, it is not clear how to overcome the long incubation delay during ALD on certain substrates that seem to resist activation.[9] Likewise, extending the ALD concept to the extreme case of 2D materials will require detailed understanding of how surface reactions self-terminate.

Given the difficulty in experimentally characterising transient reaction intermediates in sub-monolayer coverage, it is not surprising that density functional theory (DFT) simulations are increasingly being employed to investigate reaction scenarios.[10] Many DFT studies have considered the reactive adsorption of precursor molecules and desorption of protonated

ligands, which are the major mechanistic steps during the ALD of metal oxides. Initially for reasons of computational expediency, the typical model has consisted of a single precursor molecule adsorbing onto a surface saturated with complementary fragments of the other precursor. Clearly, such a model of a single adsorbate is not designed to investigate a full layer of adsorbates saturating the surface at the end of the precursor pulse. Nevertheless, differences in reactivity have been observed as the adsorbate reacts and protonated ligands desorb. The thermodynamic driving force towards saturation can be computed[11] and the saturating species can be identified. For instance, during the $Al(CH_3)_3$ pulse of Al_2O_3 ALD, it is energetically favourable for protons from surface-OH to combine with CH_3 ligands and eliminate CH_4, continuing until the relatively stable intermediate remains with just one CH_3 ligand per Al atom at the surface.[12,13] Regardless of the availability of OH groups, the $Al{-}CH_3$ fragment resists further ligand loss because of the high surface energy of a bare Al atom. Likewise during the HfX_4 pulse of HfO_2 ALD, adsorbed Hf-X is computed to resist loss of the final ligand ($X{=}N(CH_3)_2$).[14] Terminal OH groups (coordinated by one bond to the surface) are computed to be the saturating species at the end of the H_2O pulse.[14]

Pakkanen *et al.*[15] used the Hartree-Fock method to model growth of zinc sulfide from $ZnCl_2$ and H_2S. The interaction between different numbers of $ZnCl_2$ adsorbates on the ZnS surface was considered and it was shown that a bridge or chain structure is energetically more favorable than a single adsorbate at the surface. The chain model should be favored at lower temperature, while higher temperature means increased entropy and favors single chemisorption. The chain model gives rise to activation of HCl desorption since the newly formed ZnS group combines with the surface and increases the coordination number (c.n.) of neighbouring groups.

These data thus show that the ligand-covered surface becomes inert regardless of whether the co-reagent from the previous pulse (e.g. OH) is fully depleted. However it is not yet clear what reaction processes cause these inert surfaces to become re-activated when exposed to that co-reagent in the next pulse. Explaining the kinetics of saturation and re-activation is

the goal of the present work.

In this paper, we add more complexity to the models by including the consequence of adsorbate-adsorbate interaction on the H-transfer pathway (Fig. 1). Already the earliest models showed that the energetics of by-product desorption in ALD of ZnS is strongly affected by the existence of neighbouring adsorbates, although quantitative conclusions were not possible at that time because of limited computer power.[15] Here, we show that including a reasonable selection of larger number of adsorbates modifies the rate of ligand desorption, as a consequence of a change in the rate of proton transfer. This is demonstrated for ALD processes of oxides from alkylamide, alkyl, and halide precursors that perform well in practice. We speculate that the findings are valid for other ALD processes, other chemical vapour deposition processes and other surface reactions such as those during heterogeneous catalysis.

Indeed, adsorbate-adsorbate interaction was observed before in heterogeneous catalysis. To examine the influence of co-adsorbates for ammonia synthesis, Honkala *et al.*[16] used DFT to determine activation energies while changing the adsorbates in neighbouring sites on the surface. The resulting activation energies change from 0.49 eV to 1.25 eV according to their local environment. Recently Miller *et al.*[17] used DFT to describe the influence of co-adsorbates on the activation energy for O_2 dissociation on Pt(111) and found that activation energies change from 0.24 to 0.76 eV depending on the coverage of O_2 at the surface.

However, ALD reactions involve densification. Densification is defined as the increase in density due to improved metal-oxide packing, associated with an increase in c.n. of metal and oxygen from their molecular values toward bulk solid values.[14,18] Hence, to describe the change of activation energies in different local environments, the interaction between remaining fragments in the metal pulse is considered in our models before and after densification.

Results and Discussion

Each metal precursor molecule (or fragment thereof) is surrounded by other adsorbates/fragments on the surface and we show here that these neighbours have a substantial effect on the energetics along reaction paths of a particular precursor during ALD, and hence on the kinetics, even though the atoms of the neighbours do not participate directly (either stoichiometrically or catalytically) in these reactions. We term this the "cooperative effect". This is consistent with our earlier work, where we saw a strong dependence on c.n. in the adsorption and dissociation of H_2O molecules in a cluster of remaining precursor fragments.[14] It is shown that protonation and desorption of remaining ligands is facilitated in the H_2O pulse through co-adsorption of oxygen precursors such as H_2O in a cluster of remaining precursor fragments.

Reaction kinetics of $Al(CH_3)_3/H_2O$

As seen before,[12,13] adsorption of AlX_3 (for simplicity X=CH_3) occurs at under-coordinated surface oxygen atoms (Lewis basic sites) possibly bearing H (see SI Fig. 1). In order to examine the desorption of the first ligand from adsorbed AlX_3, we calculated activation energies for proton transfer from different oxygen atoms at the surface to the carbon of the ligand (Table 1 reaction 1). The lowest activation energy is $E_a = 0.28$ eV from the anchor OH group to the carbon of the ligand. The anchor OH group is threefold coordinated (excluding H) because of bonding to the Al of adsorbed AlX_3. By contrast, the other neighbouring O are one- or two-coordinated and do not release a proton as easily to the precursor, so that the calculated activation energies are much higher (e.g. 0.74 eV). Proton transfer to the methyl group causes the dissociation of methane from the metal precursor. In other words, proton transfer to C breaks the Al−C bond. This Al simultaneously forms new bonds to another oxygen at the surface. In the standard model, adsorbate-adsorbate interaction is not considered.[12,13] This dependence of E_a on coordination of O gives a first indication of

the effect of local environment on proton transfer.

Table 1: **Reaction routes for proton transfer, ligand dissociation, and ligand exchange with oxygen**

label	reaction	E_a (eV)	ΔE (eV)
1	$AlX_3(s) + OH(s)(c\cdot n\cdot{=}3) \longrightarrow AlX_2(s) + O(s)(c\cdot n\cdot{=}3) + HX(g)$	0.28	-0.78
2	$2\,AlX_2(s) + OH(s)(c\cdot n\cdot{=}2) \longrightarrow AlX_2(s) + AlX(s) + O(s)(c\cdot n\cdot{=}2) + HX(g)$	0.34	-1.78
3	$AlX_2(s) + AlX(s) + OH(s)(c\cdot n\cdot{=}3) \longrightarrow AlX(s) + AlX(s) + O(s)(c\cdot n\cdot{=}3) + HX(g)$	0.26	-0.58
4	$AlX(s)(c\cdot n\cdot{=}4) + OH(s)(c\cdot n\cdot{=}3) \longrightarrow Al(s)(c\cdot n\cdot{=}3) + O(s)(c\cdot n\cdot{=}3) + HX(g)$	1.47*	+1.47
5	$3\,AlX(s) + H_2O(s) \longrightarrow 2\,AlX(s) + Al(s) + OH(s) + HX(g)$	0.52	-1.54
6	$3\,AlX(s) + 2\,H_2O(s) \longrightarrow 2\,AlX(s) + Al(s) + H_2O(s) + OH(s) + HX(g)$	0.00	-1.12
7	$2\,HfX_2(s) + OH(s)(c\cdot n\cdot{=}3) \longrightarrow HfX_2(s) + Hf(HX)X + O(s)(c\cdot n\cdot{=}3)$	0.64	-0.86
8	$2\,Hf(HX)(HX)(s) \longrightarrow Hf(HX)(HX)(s) + Hf(HX) + HX(g)$	0.18*	+0.18
9	$HfHX(s)(c\cdot n\cdot{=}5) \longrightarrow Hf(s)(c\cdot n\cdot{=}4) + HX(g)$	1.74*	+1.74
10	$4\,HfX(s) + H_2O(s) \longrightarrow 3\,HfX(HfHX)(s) + OH(s)$	0.00	-2.24
11	$HfHX(s)(c\cdot n\cdot{=}7) \longrightarrow Hf(s)(c\cdot n\cdot{=}6) + HX(g)$	0.56	-0.14
12	$4\,HfCl_4(s) + 4\,H_2O(s) + H_2O(g) \longrightarrow 3\,HfCl_4(s) + 4\,H_2O(s) + HfCl_3(s) + OH(s) + HCl(g)$	0.00	-1.14
13	$3\,HfCl_2(s) + OH(s)(c\cdot n\cdot{=}3) \longrightarrow 2\,HfCl_2(s) + Hf(HCl)Cl(s) + O(s)(c\cdot n\cdot{=}3)$	0.00	
14	$2\,HfCl_2(s) + Hf(HCl)Cl(s) \longrightarrow 2\,HfCl_2(s) + HfCl(s) + HCl(g)$	0.13	-1.23

ΔE is energy difference and E_a is activation energy. X=CH_3 and N$(CH_3)_2$ for Al and Hf respectively.
* In these cases, E_a has been set equal to ΔE for dissociation, as no minimum was detected on the dissociation channel and as NEB calculations of E_a were subject to DFT errors at large distances.

Next, a single AlX_2 was considered at the surface. We attempted to transfer the proton of a low coordinated OH group to the carbon, but no such minimum could be found and the transferred proton returned spontaneously to the oxygen. Hence, the second desorption of HX does not occur in this situation. By contrast, desorption of HX from AlX_2 was observed in calculations by Elliott and Greer,[12] but that model used higher OH coverage and thus higher-coordinated OH. In order to check the effect of cooperation between the remaining fragments on the second HX desorption, we considered two clusters. First, we assume that $2\,AlX_2$ are adsorbed in close proximity and find that the activation energy for proton transfer from three-coordinated oxygen to carbon is 0.34 eV (Table 1 reaction 2). Second, the fragments AlX_2 and AlX are considered beside each other (Fig. 1a). The activation energy for proton transfer from the densified OH to C of AlX_2 is 0.26 eV due to coordination of this OH to AlX in its neighbourhood (Table 1 reaction 3). The densified OH group is three-coordinated again (excluding H). Desorption of the last X from AlX is an endothermic reaction in which $E_a = 1.47$ eV is required as activation energy (Table 1 reaction 4), regardless of the coordination of OH.

We see therefore that adsorption of AlX_3 makes the surface OH more acidic at the

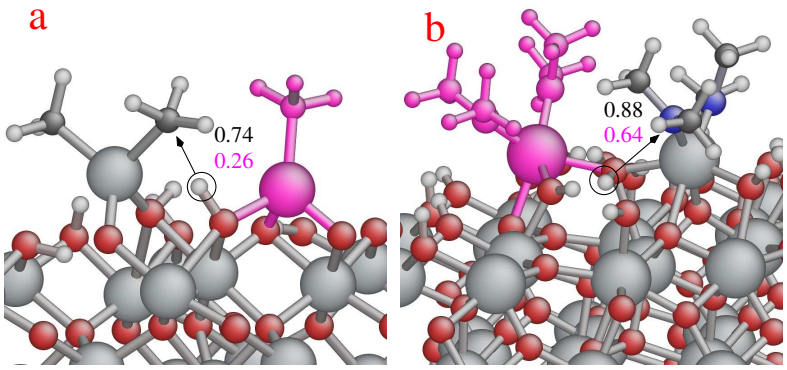

Figure 1: The presence of a remaining fragment (pink atoms) in the neighbourhood of the ligand creates a highly facilitative environment for proton transfer from the surface oxygen to the ligand. The second fragment (pink atoms) does not participate directly in proton transfer but does increase the c.n. of the central surface oxygen. Hence, the proton of the OH group becomes more acidic and the activation energy for proton transfer (given in eV) decreases significantly. (a) Growth of Al_2O_3 from $Al(CH_3)_3/H_2O$, (b) Growth of HfO_2 from $Hf(N(CH_3)_2)_4/H_2O$ (red = O, blue = N, white = H, large gray = Al or Hf, and small gray = C).

adsorption site only, which is an example of the cooperative effect. Hence, proton transfers to the ligands, with consequent ligand desorption, are facilitated indirectly through additional incoming metal precursors. After first desorption of HX, space is freed up for the smaller remaining fragments AlX_2 and AlX to coordinate to multiple surface O and OH and the rate of transfer of H from these sites to the ligands increases significantly (Fig. 1a). Therefore, the rate of ligand desorption also increases significantly for the second HX. Desorption of the last HX from AlX is computed to be relatively difficult, regardless of the acidity of OH, which makes it a less probable reaction at low temperature. Hence, it is most likely that the reactions terminate at an AlX covered surface. In this circumstance, the surface is depleted of low coordinated oxygen and fully saturated by the low coordinated metal precursors. Therefore, the surface becomes unreactive to further incoming metal precursors.

We now investigate the H_2O pulse. As mentioned above, the most probable surface species at low temperature at the end of the AlX_3 pulse would be AlX. However, we find that a single AlX cannot dissociate the incoming H_2O molecule during the water pulse (similar to

the alkylamide[14]). This is also reported for the different starting surface by Delabie *et al.*[19] This seems to be because there are not enough Lewis acid and base sites to dissociate the incoming H_2O molecule. Instead, a surface cluster of 3 AlX in close proximity is considered. To examine the influence of cooperation between the incoming H_2O molecules and remaining precursor in the cluster, one and two H_2O molecules are added to the cluster and then the activation energy for proton transfer from the incoming H_2O molecule to the carbon of the remaining ligands is calculated (see SI Fig. 2).

For the first incoming H_2O molecule in the H_2O pulse, $E_a = 0.52$ eV is required for its dissociation as it adsorbs (Table 1 reaction 5). Transfer of the proton to the methyl group of $Al{-}CH_3$ causes dissociation immediately as methane. The arrival of a second H_2O molecule makes the proton transfer barrierless (Table 1 reaction 6). These H_2O adsorption and CH_4 desorption processes are found to be exothermic. Similar but less striking results are seen for H_2O dissociation onto a cluster of 2 AlX.

We conclude that creation of such a cluster of fragments (e.g. 3 AlX) is a required step for dissociative adsorption of H_2O with consequent methane desorption at low temperature. The existence of remaining precursor fragments seems to make the surface oxygen near the cluster more Brønsted acidic than similar oxygen near a single AlX. In this situation, at the start of the H_2O pulse, the surface is depleted of protons and so the incoming H_2O is the source of protons for basic surface oxygen. Hence, the incoming H_2O molecule can be easily adsorbed and dissociated ($E_a = 0.52$ eV) in the cluster. With arrival of one more H_2O molecules the proton transfer barrier decreases even further ($E_a = 0.0$), indicating that cooperation also takes place between H_2O molecules in the H_2O pulse. This agrees with the experimental observation that ALD of Al_2O_3 from AlX_3/H_2O is possible at low temperatures.[7] At saturation, the surface is left with aluminum and oxygen atoms with c.n. similar to that in the bulk, which are therefore unreactive to incoming H_2O molecules. The surface is also terminated with low-coordinated OH groups at the end of the H_2O pulse, which are inert to the incoming H_2O molecules. The reactivity of OH group is to make

chemical bond with the metal of incoming precursor in the next pulse.

Reaction kinetics of $Hf(N(CH_3)_2)_4/H_2O$

ALD reactions for the case of alkylamide are different from the case of alkyl. As shown before,[14] desorption of HX (here X=$N(CH_3)_2$) from HfX_4 does not occur through single proton transfer since protonated amines can remain bound to the Hf centre. Once multiple proton transfer from the surface oxygen to the nitrogen of alkylamines occurs, desorption of HX commences. Due to steric repulsion between alkylamide groups, no cooperation between the precursor fragments is observed in the initial adsorbed state before densification.[20]

In order to examine the cooperation between the remaining (densified) precursors, we considered two neighbouring HfX_2 fragments (see Fig. 1b and SI Fig. 3) and compared activation energies for proton transfer and HX desorption with those for a single HfX_2. The activation energy for proton transfer from the OH group bridging two HfX_2 fragments is 0.64 eV (Table 1 reaction 7). The previously reported value[14] for a single HfX_2 was E_a = 0.88 eV. Using the computed E_a in the Arrhenius equation at 500 K, we see that the rate of proton transfer from the surface oxygen atoms to the nitrogen of the ligands is 3 orders of magnitude greater due to the presence of the other precursor fragment (Fig. 1b).[14] This also has the effect of increasing the probability of protonation of the remaining ligands. The protonation of alkylamides is an exothermic reaction.[14] Due to protonation of all ligands and repulsion between the remaining fragments, the activation energy for dissociation of HX from 2 Hf(HX)(HX) is decreased from 0.30 eV (previous reported value)[14] to 0.18 eV (Table 1 reaction 8). This reflects a weakening of Hf−N bonding when the ligands are protonated (the average Hf−N distance changes from 2.0 to 2.4 Å).

To summarize the behaviour of the alkylamide precursor during the metal pulse: the more the remaining precursor fragments densify to surface oxygen, the faster proton transfer to the remaining precursors occurs. This is because forming more bonds between precursor fragments and surface OH makes the OH proton more acidic.[14] Therefore, the surface oxygen

atoms near a cluster of fragments release protons that diffuse to the remaining ligands (Fig. 1b). In addition to increasing the rate of proton transfer through densification, repulsion between the remaining ligands facilitates the desorption of protonated ligands. Therefore, as in the $Al(CH_3)_3$ case, both proton transfer and ligand desorption are facilitated through densification of oxygen to metal.

As seen before,[14,20] surface-bound HfX is the most energetically and statistically probable species after the Hf pulse, regardless of the availability of protons. The last desorption of HX from a single HfX is endothermic with an activation energy of 1.74 eV (Table 1 reaction 9). At the end of the metal pulse therefore, the surface becomes saturated with ligands and inert to further adsorption of metal precursor, similar to the Al_2O_3 case above, but is chemically activated to the H_2O molecule, which is discussed next.

To examine the cooperation between the remaining ligands to dissociate an incoming H_2O molecule in the H_2O pulse, we considered 4 HfX as a typical example of the remaining ligands from the metal pulse (Fig. 2 and SI Fig. 4). The first H_2O molecule arriving into the cluster is easily dissociated by proton transfer to the neighbouring basic atoms (nitrogen here) and this dissociation is barrierless (Table 1 reaction 10). The surface oxygen atoms involved in the 4 HfX cluster are stronger Brønsted basic active sites than those near a single HfX and the nitrogen atoms of ligands in the cluster are stronger Brønsted basic active sites than those of a single HfX. Hence, the incoming H_2O molecule is readily adsorbed and dissociated (i.e. dissociative adsorption of H_2O) (Fig. 2).

Through the introduction of more H_2O molecules into the cluster, Hf of the remaining precursor fragment obtains a higher c.n from the oxygen of the incoming H_2O molecules. This results in the exothermic desorption of HX with a lower activation energy (0.56 eV) (Table 1 reaction 11). Adsorption of H_2O thus reactivates the surface towards elimination of ligands. Hence, the remaining alkylamines are replaced with OH groups and the surface is left with a bulk-like coordination of hafnium (c.n. = 6-8) and oxygen (c.n. = 3-4) atoms, along with low coordinated OH, at the end of the H_2O pulse.[20] We conclude that the surface

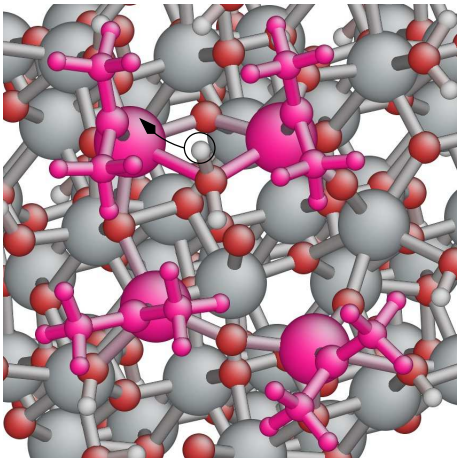

Figure 2: Dissociative adsorption of the incoming H_2O molecule in the cluster of 4 HfX (pink atoms). In this situation, the H_2O molecule is coordinatively saturated. Hence, the adsorbed H_2O molecule is readily dissociated by Brønsted basic sites ($E_a = 0.0$ eV).

has become re-activated to the incoming metal precursor of the next pulse in the ALD cycle.

Reaction kinetics of $HfCl_4/H_2O$

One of the most commercially important ALD processes is the deposition of HfO_2 from $HfCl_4$ and H_2O. So far, the overall computed ALD reactions from halide precursors have been reported in the literature to be endothermic.[21] In other words, no intrinsic driving force for the steps of the growth reaction has been discovered yet. As reported before, adsorption of the hafnium chloride precursor is energetically favorable and a dative chemical bond between the hafnium of the adsorbing $HfCl_4$ precursor and a surface oxygen atom is created. It was shown that the adsorption energy depends on water coverage. As water coverage increases, the metal precursor interacts with multiple surface adsorption sites.

Our calculations for a dense, smooth layer of surface oxygen show that after adsorption of $HfCl_4$ the surface protons do not diffuse to the chloride of adsorbed precursor, because there are large barriers ($E_a \geq 1.0$ eV). Therefore, we suppose that the intact $HfCl_4$ molecule can be the energetically favorable surface species at the end of the metal precursor pulse. Once the surface is covered by a monolayer of halide precursors, creation of chemical bonds

between the surface oxygen and the metal of the precursor is stopped.

However, we observe in simulation that the presence of other $HfCl_4$ allows further adsorption of $HfCl_4$ through the creation of Hf−Cl−Hf bridges, so that chains of $HfCl_4$ are made at the surface. This agrees with the Zn−Cl−Zn chains computed by Pakkanen *et al.* at the Hartree-Fock level.[15] This suggests that multiple mono-layers of adsorbate are formed that are physically and chemically bonded to each other and to the surface (see SI Fig. 5). In this situation, we expect that the number of layers depends on the ALD temperature: since adsorbates are physisorbed at the top layers, increasing temperature should cause them to desorb. Hence, a lower growth rate can be expected at high temperature,[22] while at low temperature growth may not be self-limiting.

We therefore investigate whether ligand elimination can take place in the H_2O pulse. In order to examine the effect of cooperation between the incoming H_2O molecules on desorption of remaining ligands from $HfCl_4$ clusters, we considered 4 $HfCl_4$ beside each other and considered adsorption and optimization of H_2O molecules one by one. Initially, a chain of $HfCl_4$ at the surface linked by bridging chloride is observed with Hf c.n. ranging from 4 to 6. At the beginning, no evidence of H_2O dissociation or HCl desorption is observed since E_a is still high. However, with the arrival of more H_2O molecules into the cluster the activation energy drops, until with sufficient H_2O (e.g. here 5 H_2O molecules), spontaneous proton transfer to the chloride is observed (Fig. 3). Adsorption of a H_2O molecule becomes exothermic for the fifth adsorption (-1.14 eV, Table 1 reaction 12). Thus, with the start of the H_2O pulse, dissociation of HCl commences. The transferred protons in HCl come directly from the incoming H_2O molecules and not from surface OH. After the first HCl desorption, the remaining halide precursor $HfCl_3$ is not densified into the surface.

As mentioned above, several layers of adsorbate are expected during the metal pulse at low temperature . In low temperature ALD therefore, the by-product HCl may be buried in the growing layers and this may cause chlorine contamination and/or etching in the films.[22] The physisorbed layers of $HfCl_4$ are probably thinner at high temperature than at low

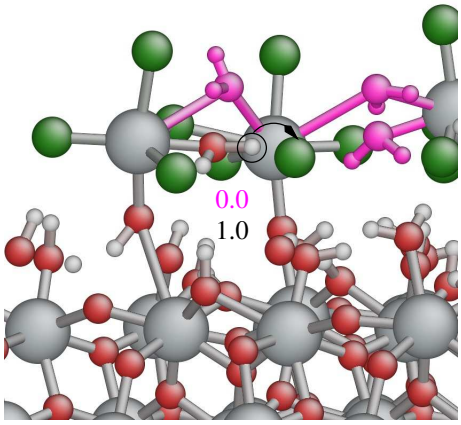

Figure 3: Due to adsorption of multiple H_2O molecules (pink atoms) into the cluster of remaining $HfCl_x$ fragments, the activation energy for proton transfer (given in eV) decreases significantly. (red = O, green = Cl, white = H, large gray = Hf).

temperature. Hence, the by-product HCl can be more easily desorbed at high temperature and less contamination is observed.[22]

In order to check this cooperative effect, a cluster of 3 $HfCl_2$ is considered (see SI Fig. 6). Bridging oxygen either from the oxygen precursor or from the surface allows the Hf of the metal precursor to obtain higher c.n.. In this cluster, because the densified oxygen is fully coordinated (c.n. = 3) to Hf, it readily donates its proton. Hence proton transfer to the chloride is barrierless (Table 1 reaction 13). The activation energy for a third HCl desorption is also very low, at 0.13 eV (Table 1 reaction 14).

Dissociation of HCl from the remaining chloride fragments (e.g. $HfCl_2$) is only possible once the hafnium becomes fully coordinated (5 or 6 coordinated). At the same time, the surface oxygen or the incoming oxygen precursor should also be fully coordinated in order to release protons for transfer to the remaining chloride. These two conditions are not frequently fulfilled during the $HfCl_4$ pulse, and so adsorbates like $HfCl_4$ and $HfCl_3$ predominate as the saturated surface at the end of the $HfCl_4$ pulse. Including the cooperative effect between adsorbates, the calculated activation energies are lower than in the simple model and the reactions during the H_2O pulse are now found to be exothermic. The surface OH are seen to

become more acidic and the remaining ligands (Cl) more basic due to the cooperative effect. In such circumstances, the rate of proton transfer from coordinatively saturated OH groups to chloride increases. Hence, the remaining chlorides are replaced with OH groups and the surface is left with bulk-like hafnium and oxygen atoms, as well as OH-termination at the end of the H_2O pulse. The low coordinated OH groups re-activate the surface towards the metal precursor of the next pulse.

Conclusion

We now draw some general conclusions. During the metal pulse (right hand side of Fig. 4), Lewis acidic precursor MX_n adsorbs onto a basic terminal OH group. Formation of the new M−O bond makes O less basic, but makes H at the anchor site more acidic. Neighbouring MX fragments and fresh MX fragments reduce the activation energy for H-transfer (the co-operative effect). Hence, the rate of proton transfer from the surface oxygen to the remaining ligands increases significantly and causes desorption of the ligands. Loss of ligands allows precursor fragments to densify into the surface, further increasing the mutual coordination of metal and oxygen. Adsorption and elimination reactions continue until all O has become fully coordinated to M, retains no more H and is inert with respect to further adsorption of metal precursor. This explains the self-limiting chemistry of ALD. In the bulk, M and O c.n. are exactly balanced (when adjusted for stoichiometry), but at the surface there is now an excess of M, which remains relatively under-coordinated (Lewis acidic) and therefore retains ligands (lower side of Fig. 4). The ligand-covered surface is thus a consequence of the saturation of O coordination.

This surface is exposed to H_2O during the O pulse (left hand side of Fig. 4), where H_2O functions as a Lewis base. Co-adsorptions of H_2O in a cluster of the remaining precursor fragments increases the c.n. of the metal atoms and facilitates dissociation of H_2O. Therefore, further protonation and desorption of the ligands can occur.

In other words, the net effect is transfer of basicity from O of adsorbing H_2O to X of desorbing HX, and quenching of the acidity of surface M as its c.n. increases. Eventually, when coordination of M approaches bulk values, no further chemisorption of H_2O can take place and the surface is saturated (self-limiting ALD). At this point, excess O is present as low-coordinated terminal OH, and is therefore Lewis basic, ready for the next cycle (upper side of Fig. 4).

The presence of minor ligands (e.g. AlX) (upper side of Fig. 4) should be observed, once the creation of a cluster of precursor fragments is not fulfilled. Uneliminated ligands such as these may be a source of impurities in the film. In addition, we predict that isolated adsorbate fragments (e.g. single AlX not in a cluster) should be inert towards elimination during the H_2O pulse (upper side of Fig. 4) and thus should be detected experimentally. The cooperative effect is the crucial feature that facilitates ligand desorption and accounts for the reaction kinetics in the ALD process.

In summary, our first-principle calculations of activation energies in different local environments on metal oxide surfaces show the central role played by coordination number. By computing complex surface models including co-adsorption precursors, we find that the reaction pathways have lower activation energy than previously reported. In some cases, these are the first reaction pathways computed to be viable at process temperatures. Undercoordinated oxygen is reactive towards adsorption of Lewis acidic metal precursors (e.g. $Al(CH_3)_3$, $Hf(N(CH_3)_2)_4$), which in turn through the cooperative effect make hydroxyl groups more Brønsted acidic. A complementary set of reactions is observed when a ligand-covered surface is exposed to H_2O, with co-adsorption activating both H_2O towards dissociation and ligands towards protonation and desorption. These findings give clear pointers for how to control the acidity/basicity of oxide surfaces, e.g. for heterogeneous catalysis. They also show how saturation of coordination number can explain the self-limiting nature of ALD, from which the unique advantages of this technique are derived.

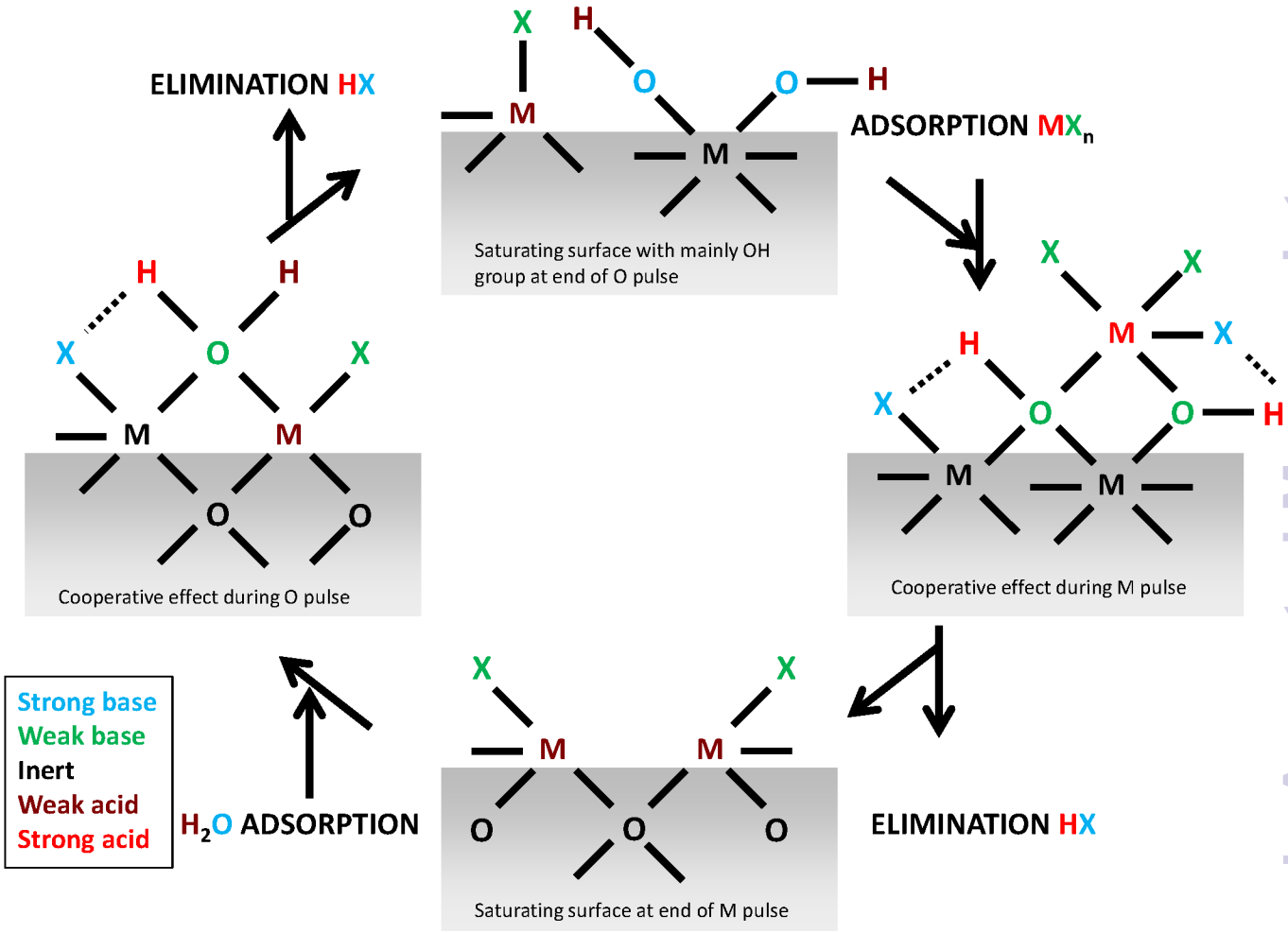

Figure 4: Schematic summarising the changes observed in DFT calculations in the apparent Lewis basicity (blue/green) and acidity (red/brown) of surface atoms during a cycle of ALD of metal oxides (M=metal, X=ligand). The types of species present at saturation are shown top and bottom, while typical intermediates during the oxygen and metal pulses are shown on the left and right respectively. 'Strong' and 'Weak' are meant as relative terms, as the absolute acidity or basicity depends on the particular system. Solid lines are indicative of coordination around M and O and dashed lines show H-transfer reactions whose activation energies are affected by the cooperative effect. As noted in the text, other types of reaction (not shown here) are also subject to a cooperative effect.

Methods

To model the growth reactions of metal oxides from $Al(CH_3)_3$ (TMA), $Hf(N(CH_3)_2)_4$ (TDMAHf), $HfCl_4$ and H_2O, self-consistent DFT[23] was used as implemented in the Vienna ab initio simulation package (VASP).[24] The technical parameters used for the Al_2O_3[12] and HfO_2[14] ALD systems can be found in the respective references. We calculated activation energies (E_a) between two minima on the potential energy hypersurface using the nudged elastic band approach[25,26] implemented in VASP. In this paper, all simulations of reactions in the metal pulse are carried out on a smooth surface of fully saturated surface oxygen. We speculate that reaction energetics and kinetics are also valid for a rough surface, if the coordination of the atoms is known.

The statistical distribution of fragments of TDMAHf precursors at the surface at the start of the O pulse is obtained from the stochastic parallel particle kinetic simulator (SPPARKS) code,[27,28] in which we have implemented ALD surface reactions as a new feature using kinetic Monte-Carlo (KMC).[20] As we have not implemented the $Al(CH_3)_3$ and $HfCl_4$ chemistries into the KMC yet, we assume that they exhibit roughly the same statistical distribution as TDMAHf in terms of number of remaining fragments at the end of the metal pulse.

Acknowledgement

Financial support from the Science Foundation Ireland (SFI)-funded strategic research cluster 'Functional Oxides and Related Materials for Electronics' (FORME) and 'ALDesign' project , are gratefully acknowledged. The authors wish to acknowledge the SFI/HEA Irish Centre for High-End Computing (ICHEC) for the provision of computational facilities and support. The authors declare that they have no competing financial interests.

Supporting Information Available

Full details of computed reaction pathways are given in Supporting Information. All modelling coordinates are included in Supporting Information.

This material is available free of charge via the Internet at `http://pubs.acs.org/`.

References

1. Geim, A. K.; Novoselov, K. S. The rise of graphene. *Nature Materials* **2007**, *6*, 183–191.

2. Perkins, F. K.; Friedman, A. L.; Cobas, E.; Campbell, P. M.; Jernigan, G. G.; Jonker, B. T. Chemical Vapor Sensing with Monolayer MoS2. *Nano Letters* **2013**, *13*, 668–673.

3. Wang, L.; Travis, J. J.; Cavanagh, A. S.; Liu, X.; Koenig, S. P.; Huang, P. Y.; George, S. M.; Bunch, J. S. Ultrathin Oxide Films by Atomic Layer Deposition on Graphene. *Nano Letters* **2012**, *12*, 3706–3710.

4. Leskelä, M.; Ritala, M. Atomic Layer Deposition Chemistry: Recent Developments and Future Challenges. *Angewandte Chemie International Edition* **2003**, *42*, 5548–5554.

5. Miikkulainen, V.; Leskela, M.; Ritala, M.; Puurunen, R. L. Crystallinity of inorganic films grown by atomic layer deposition: Overview and general trends. *Journal of Applied Physics* **2013**, *113*, 021301.

6. Hausmann, D. M.; Kim, E.; Becker, J.; Gordon, R. G. Atomic Layer Deposition of Hafnium and Zirconium Oxides Using Metal Amide Precursors. *Chemistry of Materials* **2002**, *14*, 4350–4358.

7. Groner, M. D.; Fabreguette, F. H.; Elam, J. W.; George, S. M. Low-Temperature Al2O3 Atomic Layer Deposition. *Chemistry of Materials* **2004**, *16*, 639–645.

8. Knapas, K.; Ritala, M. In Situ Studies on Reaction Mechanisms in Atomic Layer Deposition. *Critical Reviews in Solid State and Materials Sciences* **2013**, *38*, 167–202.

9. Hämäläinen, J.; Ritala, M.; Leskelä, M. Atomic Layer Deposition of Noble Metals and Their Oxides. *Chemistry of Materials* **2014**, *26*, 786–801.

10. Elliott, S. D. Atomic-scale simulation of ALD chemistry. *Semiconductor Science and Technology* **2012**, *27*, 074008.

11. Elliott, S. D. Predictive process design: a theoretical model of atomic layer deposition. *Computational Materials Science* **2005**, *33*, 20 – 25,.

12. Elliott, S. D.; Greer, J. C. Simulating the atomic layer deposition of alumina from first principles. *J. Mater. Chem.* **2004**, *14*, 3246–3250.

13. Xu, Y.; Musgrave, C. B. A DFT Study of the Al2O3 Atomic Layer Deposition on SAMs:£ Effect of SAM Termination. *Chemistry of Materials* **2004**, *16*, 646–653.

14. Shirazi, M.; Elliott, S. D. Multiple Proton Diffusion and Film Densification in Atomic Layer Deposition Modeled by Density Functional Theory. *Chemistry of Materials* **2013**, *25*, 878–889.

15. Pakkanen, T. A.; Nevalainen, V.; Lindblad, M.; Makkonen, P. Surface models for ZnS thin films: Theoretical studies on the mechanism of the growth of zinc sulfide by atomic layer epitaxy techniques. *Surface Science* **1987**, *188*, 456 – 474.

16. Honkala, K.; Hellman, A.; Remediakis, I. N.; Logadottir, A.; Carlsson, A.; Dahl, S.; Christensen, C. H.; Nørskov, J. K. Ammonia Synthesis from First-Principles Calculations. *Science* **2005**, *307*, 555–558.

17. Miller, D. J.; Oberg, H.; Naslund, L.-A.; Anniyev, T.; Ogasawara, H.; Pettersson, L. G. M.; Nilsson, A. Low O[sub 2] dissociation barrier on Pt(111) due to adsorbate–adsorbate interactions. *The Journal of Chemical Physics* **2010**, *133*, 224701.

18. Olivier, S.; Ducere, J.-M.; Mastail, C.; Landa, G.; Esteve, A.; Rouhani, M. D. Insights into Crystalline Preorganization of Gas-Phase Precursors: Densification Mechanisms. *Chemistry of Materials* **2008**, *20*, 1555–1560.

19. Delabie, A.; Sioncke, S.; Rip, J.; Van Elshocht, S.; Pourtois, G.; Mueller, M.; Beckhoff, B.; Pierloot, K. Reaction mechanisms for atomic layer deposition of aluminum oxide on semiconductor substrates. *Journal of Vacuum Science and Technology A* **2012**, *30*.

20. Shirazi, M.; Elliott, S. D. Atomistic kinetic Monte Carlo study of atomic layer deposition derived from density functional theory. *Journal of Computational Chemistry* **2014**, *35*, 244–259.

21. Mukhopadhyay, A. B.; Musgrave, C. B.; Sanz, J. F. Atomic Layer Deposition of Hafnium Oxide from Hafnium Chloride and Water. *Journal of the American Chemical Society* **2008**, *130*, 11996–12006.

22. Delabie, A.; Caymax, M.; Brijs, B.; Brunco, D.; Conard, T.; Sleeckx, E.; Ragnarsson, L.-A.; Van Elshocht, S.; De Gendt, S.; Heyns, M. Growth Studies and Reaction Mechanism of the Atomic Layer Deposition of Hafnium Oxide. *ECS Transactions* **2006**, *1*, 433–446.

23. Kohn, W.; Becke, A. D.; Parr, R. G. Density Functional Theory of Electronic Structure. *The Journal of Physical Chemistry* **1996**, *100*, 12974–12980.

24. Kresse, G.; Hafner, J. *Ab initio* molecular dynamics for liquid metals. *Phys. Rev. B* **1993**, *47*, 558–561.

25. Henkelman, G.; Uberuaga, B. P.; Jonsson, H. A climbing image nudged elastic band method for finding saddle points and minimum energy paths. *The Journal of Chemical Physics* **2000**, *113*, 9901–9904.

26. Henkelman, G.; Jonsson, H. Improved tangent estimate in the nudged elastic band method for finding minimum energy paths and saddle points. *The Journal of Chemical Physics* **2000**, *113*, 9978–9985.

27. Slepoy, A.; Thompson, A. P.; Plimpton, S. J. A constant-time kinetic Monte Carlo algorithm for simulation of large biochemical reaction networks. *The Journal of Chemical Physics* **2008**, *128*, 205101.

28. Bortz, A.; Kalos, M.; Lebowitz, J. A new algorithm for Monte Carlo simulation of Ising spin systems. *Journal of Computational Physics* **1975**, *17*, 10 – 18.